ELSEVIER

materialstoday

www.materialstoday.com SEPTEMBER 2007 | VOLUME 10 | NUMBER 9

At breaking point

Deformation and fracture from the nano to macroscale

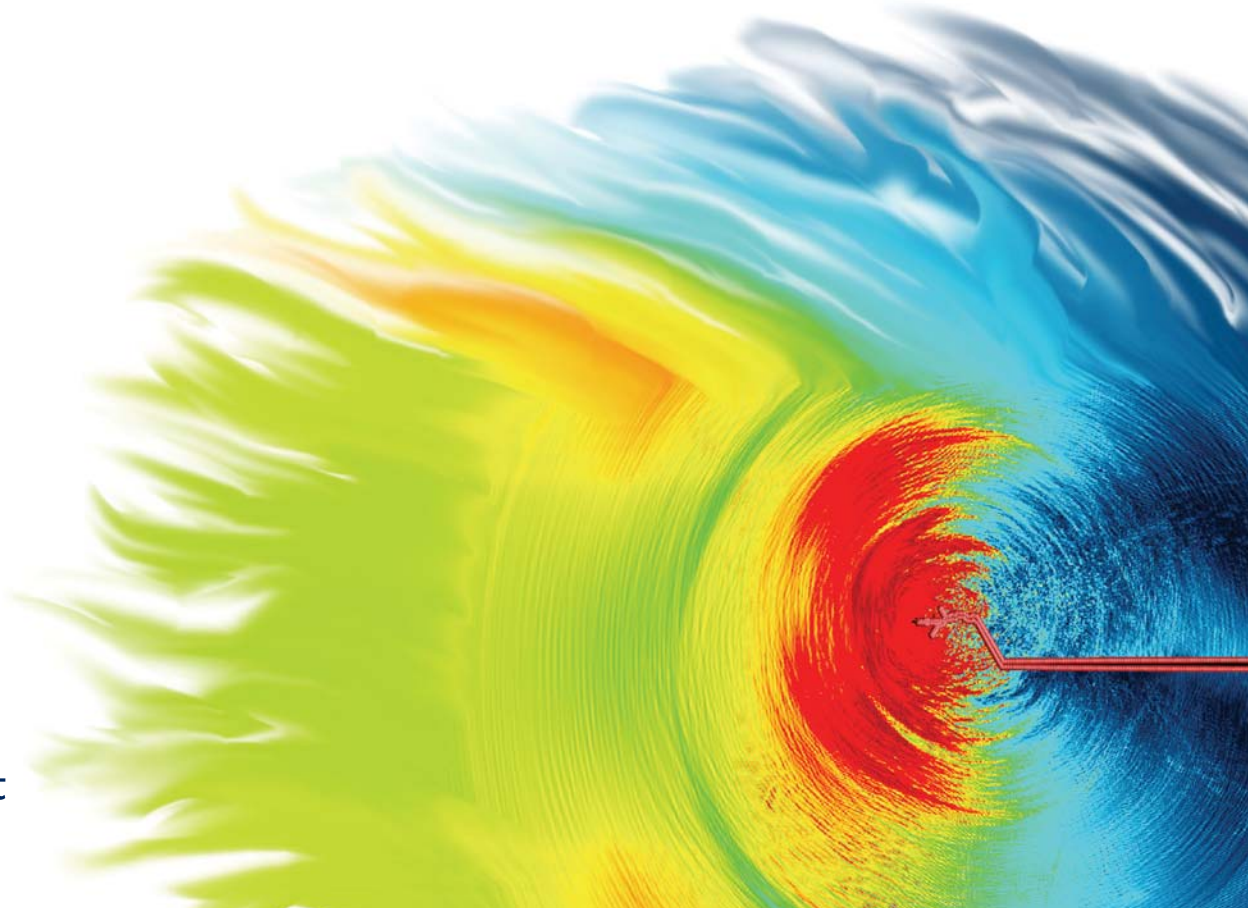

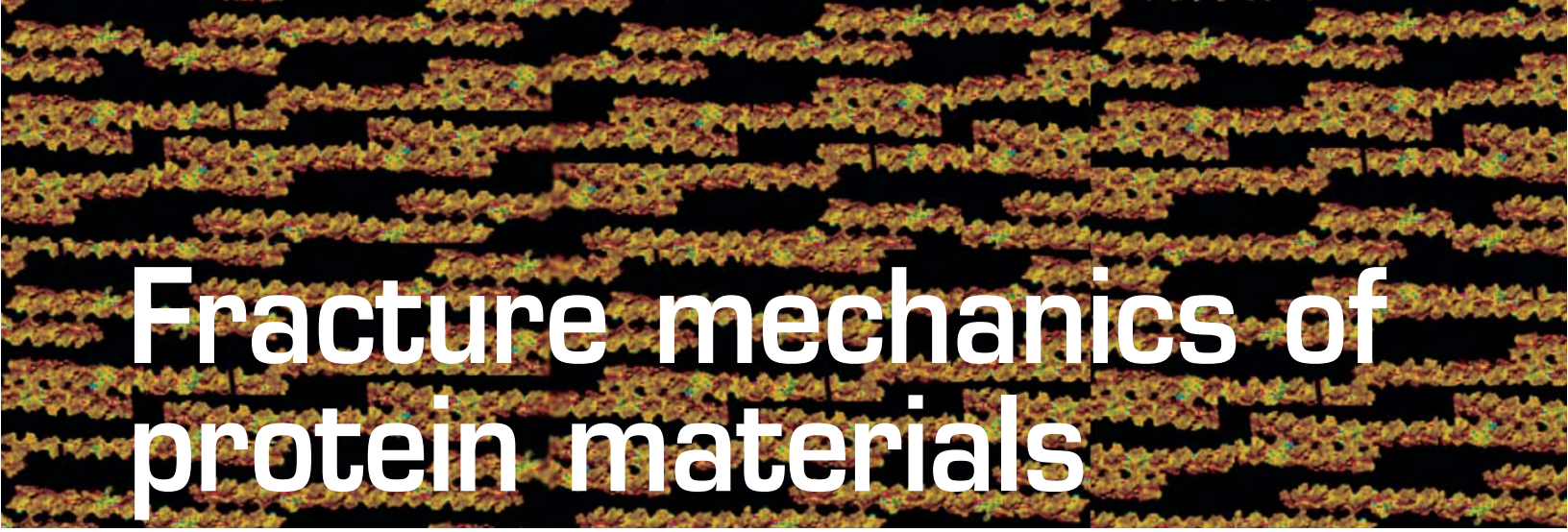

Fracture mechanics of protein materials

Proteins are the fundamental building blocks of a vast array of biological materials involved in critical functions of life, many of which are based on highly characteristic nanostructured arrangements of protein components that include collagen, alpha helices, or beta sheets. Bone, providing structure to our body, or spider silk, used for prey procurement, are examples of materials that have incredible elasticity, strength, and robustness unmatched by many synthetic materials. This is mainly attributed to their structural formation with molecular precision. We review recent advances in using large-scale atomistic and molecular modeling to elucidate the deformation and fracture mechanics of vimentin intermediate filaments (IFs), which are hierarchical self-assembled protein networks that provide structure and stability to eukaryotic cells. We compare the fracture and failure mechanisms of biological protein materials (BPMs) with those observed in brittle and ductile crystalline materials such as metals or ceramics. Our studies illustrate how atomistic-based multiscale modeling can be employed to provide a first principles based material description of deformation and fracture, linking nano- to macroscales.

Markus J. Buehler* and Theodor Ackbarow

Laboratory for Atomistic and Molecular Mechanics, Massachusetts Institute of Technology, Department of Civil and Environmental Engineering, 77 Massachusetts Ave. Room 1-272, Cambridge, MA, 02139, USA

**E-mail: mbuehler@MIT.EDU*

When materials are deformed, they display a small regime in which deformation is reversible or elastic[1–3]. Once the forces on the material reach a certain level, deformation becomes irreversible and remains even after the load is removed. This is referred to as the plastic regime[1–3]. Plastic deformation is typically followed by fracture, when the material breaks and fails. Many

ISSN:1369 7021 © Elsevier Ltd 2007

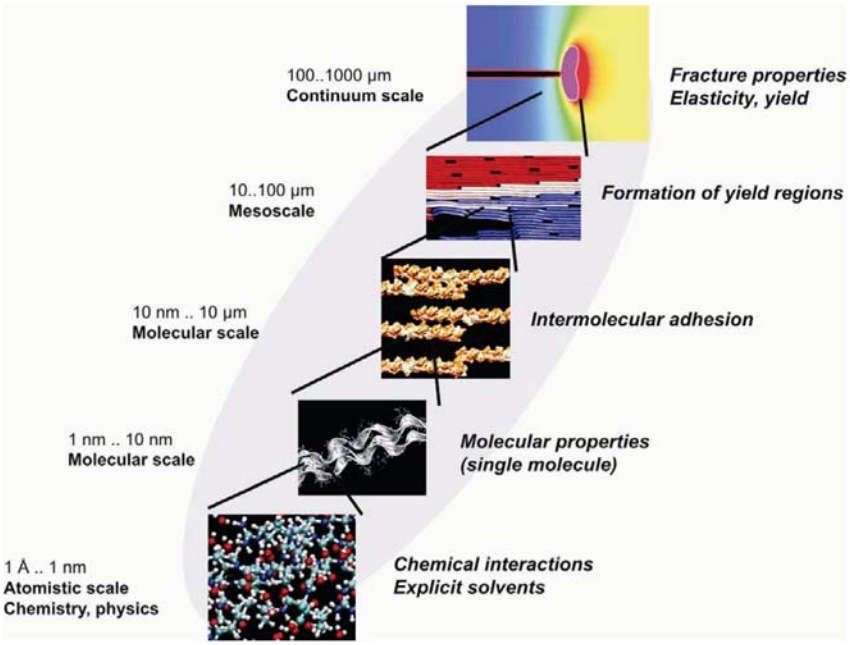

Fig. 1 Overview of different material scales, from nano to macro, here exemplified for collagenous tissue[5–9]. BPMs such as collagen, skin, bone, spider silk, or cytoskeletal networks in cells feature complex, hierarchical structures. The macroscopic mechanical material behavior is controlled by the interplay of properties throughout various scales. In order to understand deformation and fracture mechanisms, it is crucial to elucidate atomistic and molecular mechanisms at each scale.

materials, including metals, ceramics, polymers, and biological tissue show this generic behavior[1–3]. However, the details of the response to mechanical load depend on the atomic and molecular makeup of the material; from nano- to macroscales (see Fig. 1).

For example, ductile metals such as Cu or Ni can rather easily undergo large permanent (or 'plastic') deformation without breaking[3]. On the other hand, brittle materials like glass or Si cannot easily be deformed, but instead fracture rapidly once the applied load exceeds a threshold value[1]. Conversely, BPMs such as the cell's cytoskeleton[4] or collagen networks in tendon or bone[5–10] represent intriguing protein networks that can dynamically adapt to load application by self-organization and self-arrangement. They develop stronger filaments when needed and disposing of those that do not contribute to the strength, making the material utilization more efficient and robust against failure overall.

Understanding the origin of deformation and fracture of materials has fascinated generations of material scientists. Currently, a major challenge is the elucidation of mechanisms in increasingly complex materials – materials that consist of multiple components or multiple hierarchies, or those whose atomic nano- and microstructures contain a concurrent interplay of a variety of chemical bonds. An important concept in understanding the deformation and failure properties of materials is the underlying fundamental atomic mechanisms[1,3,11], as illustrated in Fig. 2 for ductile materials[3], brittle materials[1], and BPMs.

While the basic deformation mechanisms of crystalline solids are relatively well understood, analogous mechanisms have only

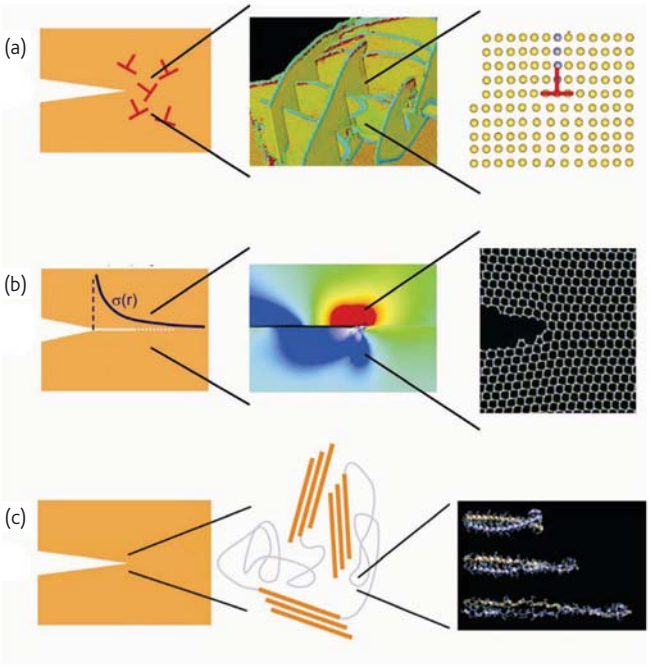

Fig. 2 Overview of the deformation and fracture behavior of different classes of materials, including (a) ductile materials[3], (b) brittle materials[1], and (c) BPMs. Each subplot shows a multiscale view of associated deformation mechanisms. In ductile materials, deformation is mediated by the creation of dislocation networks; each dislocation represents localized shear of the atomic lattice. In brittle materials, fracture occurs by the spreading of cracks, which is mediated by continuous breaking of atomic bonds. In BPMs, a complex interplay of different protein structures controls the mechanical response. At the ultrascale, the unfolding of individual protein molecules by rupture of hydrogen bonds (HBs) represents the most fundamental deformation mechanism.

recently been discovered in BPMs. Permanent plastic deformation in these materials is mediated by intermolecular slip, the unfolding of proteins[12,13], the breaking of intermolecular cross-links[14,15], or the stretching of convoluted protein chains, as has been demonstrated in multiscale simulations for collagenous materials and bone[5,6,10,15,16] for instance.

Because of the multiscale hierarchical structure of these materials, different deformation mechanisms may occur at each scale, while the inter- and intrahierarchal interactions might be of competing or reinforcing character. The most fundamental deformation mode is, however, often the breaking of weak hydrogen bonds (HBs). Even though HBs are 100 to 1000 times weaker than covalent bonds, HBs are the most important type of chemical bonds that hold together proteins, assemblies of proteins, and that control their adhesion behavior, and thereby play a vital role in controlling many biological processes. Up to now, neither a systematic classification nor fundamental theories exist for the different deformation and fracture mechanisms in BPMs.

The mechanical properties of BPMs have wide ranging implications for biology. In cells for instance, mechanical sensation is used to transmit signals from the environment to the cell nucleus or to control tissue formation and regeneration[4,17]. The structural integrity and shape of cells is controlled by the cell's cytoskeleton, which resembles an interplay of complex protein structures and signaling cascades arranged in a hierarchical fashion. The transfer of concepts observed in biology into technological applications and new material design – a field referred to as biomimetics – remains a significant challenge with, however, a potentially enormous payoff. In particular, the combination of nanostructural and hierarchical features into materials developments could lead to breakthroughs in the design of new materials.

Predictive computational experiments of deformation and fracture

Materials failure processes begin with the erratic motion of individual atoms around flaws or defects within the material. These evolve into the formation of macroscopic fractures as chemical bonds rapidly rupture, eventually compromising the integrity of the entire structure. Thus the behavior of chemical bonds under a large stretch – on a small scale – controls how structures respond to mechanical load and fail on much larger material scales, as has, for instance, been demonstrated for model materials and Si[18–21].

Fracture mechanisms in brittle and ductile materials are representative examples of an intrinsic multiscale problem that cannot be understood by considering one scale alone (see Figs. 1 and 2). Experimentation, simulation, and development of theories must therefore consider a complex interplay of mechanisms at several scales. In particular in hierarchical BPMs, the development of a rigorous understanding of deformation depends critically on the elucidation of the deformation mechanism at each scale, and how these mechanisms interact dynamically across the scales.

Hierarchical multiscale modeling

Multiscale modeling is a particularly useful approach to gain insight into these complex problems. In order to allow the best resolution at any length and time scale, a set of computational methods is integrated seamlessly, enabling one to bridge scales from nano to macro (Fig. 3).

Atomistic simulation, or molecular dynamics (MD)[22], provides a fundamental view on materials deformation – describing the patterns of fracture, yield, diffusion, and other mechanisms at resolutions that cannot yet be reached by experiments. After careful validation of these

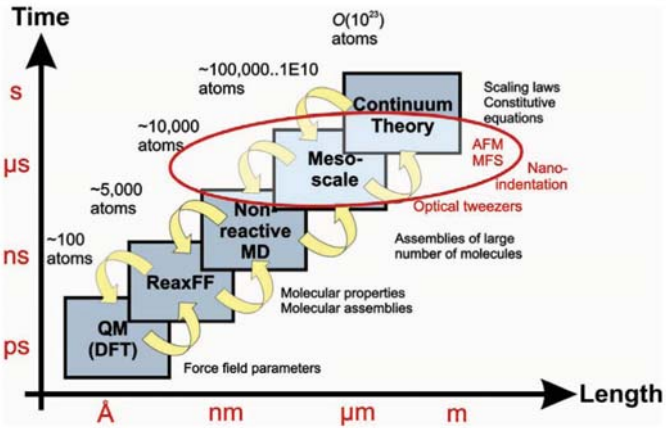

Fig. 3 Schematic of the concept of hierarchical multiscale modeling. Hierarchical coupling of different computational tools can be used to traverse throughout a wide range of length and time scales. Such methods provide a fundamental insight into deformation and fracture phenomena across various time and length scales. Handshaking between different methods enables one to transport information from one scale to another. Eventually, results of atomistic, molecular, or mesoscale simulation may feed into constitutive equations or continuum models. While continuum mechanical theories have been very successful for crystalline materials, modeling the behavior of BPMs requires statistical theories, e.g. the extended Bell theory reviewed here. Experimental techniques such as atomic force microscopy (AFM), molecular force spectroscopy (MFS), nanoindentation, or optical tweezers now overlap into atomistic and molecular approaches, enabling direct comparison of experiment and simulation.

computational models with experiments, atomistic and multiscale modeling have predictive power[23]. Predictive multiscale simulation could play an important role in science, engineering, and materials design in the coming decades.

Experimental techniques to probe ultrasmall scale material mechanics

Recent advances in experimental techniques further facilitate analyses of ultrasmall-scale material behavior. For instance, techniques such as nanoindentation, optical tweezers, or atomic force microscopy (AFM) can provide valuable insight to analyze the molecular mechanisms in a variety of materials, including metals, ceramics, and proteins[13,24–27]. A selection of experimental techniques is summarized in Fig. 3, illustrating the overlap with multiscale simulation methods.

Basics of atomistic modeling

The basic concept behind atomistic simulation via MD is to calculate the dynamic trajectory of each atom in the material, by considering their atomic interaction potentials and solving each atom's equation of motion according to $F = ma$ (where F is the force vector, m the atomic mass, and a the acceleration)[22]. Numerical integration of this equation by considering proper interatomic potentials enables simulation of a large ensemble of atoms that represents a larger material volume, albeit typically limited to several nanoseconds. The availability of interatomic potentials for a specific material is often a limiting factor in the applicability of this method.

Provided suitable interatomic potentials are available, MD is capable of directly simulating a variety of materials phenomena, for instance the response of an atomic lattice to applied loading under the presence of a crack-like defect, or the unfolding mechanisms of proteins.

In the following two sections, we briefly review atomistic simulation applied to ductile and brittle materials. We then move on to discuss the behavior of BPMs, exemplifying a theoretical and numerical approach to address the fundamental deformation mechanisms in vimentin IF networks. We conclude with a discussion and outlook, in particular highlighting similarities and differences between the classes of materials discussed here. We note that we primarily review specific research results from our own group.

Deformation of ductile materials: dislocation-mediated plasticity

Ductile materials are characterized by their ability to undergo significant plastic deformation without breaking[3]. The fundamental mechanism for this behavior is the formation of dislocations, which represent a localization of shear displacement in the atomic lattice. Instead of shearing an entire crystal homogeneously, a dislocation represents a localization of shear that propagates through the material, often nucleated at crack-like defects that represent locations of shear stress concentration[3]. Accumulation of dislocations enables materials to undergo significant shape change without breaking[3] (see Fig. 2a).

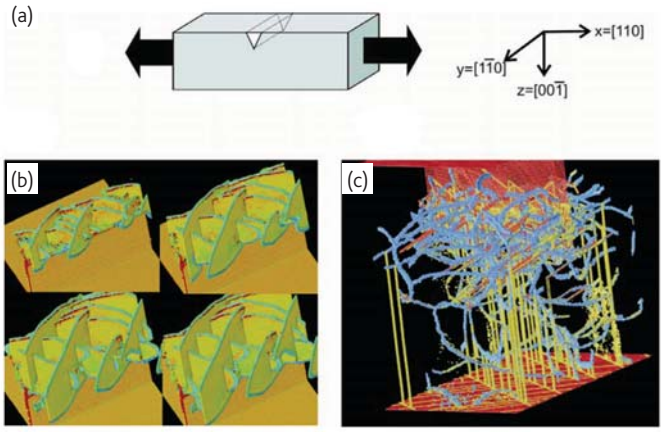

Fig. 4 (a) Tensile deformation of a Ni nanowire with a surface crack. The geometry is a nanowire of face-centered cubic Ni with a small surface crack, simulated by considering a cubic volume with 50 nm side length and periodic boundary conditions in the wire direction (x-direction). The atomic interactions are modeled using EAM[28] adapted for Ni[29]. (b) Upon increase of the tensile load to a few percent strain, dislocations start to emerge at the small surface crack because of large local shear stresses. (c) Quickly, the entire crystal is filled with a complex entanglement of dislocations. The increasing entanglement of dislocations makes it more difficult for new dislocations to nucleate and propagate into the crystal, thus making the material stronger. This effect is known as strain hardening[3].

A case study of large-scale atomistic modeling of deformation of a Ni nanowire using the embedded atom method (EAM)[28] adapted for Ni[29] is presented in Fig. 4. The EAM has become a widely used tool in the computational materials science of metals. For instance, MD simulations have significantly contributed to the understanding of deformation of nanocrystalline metals[30–32].

Brittle materials: failure by spreading of fractures

The fracture of brittle solids proceeds by the breaking of atomic bonds, leading to the formation of new material surfaces. In contrast to ductile solids, the brittle character of materials arises from the energetic favorability of bond rupture over shearing of the material[1,3]. This can be quantified by considering ratios of the stacking fault energies and surface energy, as discussed elsewhere[33,34].

Once the applied load exceeds a critical value, a brittle solid fails because of the spreading of a large number of fractures. The presence of a crack is vital for this process, since it provides a location with locally large stresses. Fig. 2b depicts the fundamental fracture mechanism of a brittle material, indicating the large stresses at the tip of the crack that cause repeated rupture of atomic bonds.

A representative case study of atomistic modeling of the fracture of Si is shown in Fig. 5, with a series of results obtained using a multiparadigm approach[20] based on the combination of the ReaxFF

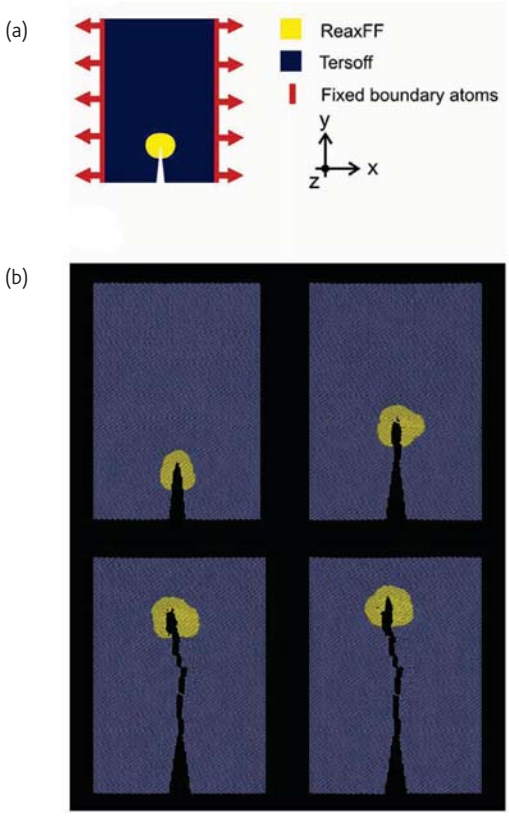

Fig. 5 Multiparadigm simulation of dynamic fracture of Si[20,21]. (a) The slab geometry is approximately 50 nm by 100 nm in plane-strain geometry (out-of-plane thickness is one unit cell), with an initial crack length a ≈ 17 nm. This model describes the fracture mechanics of Si by a combination of a simple Tersoff force field in regions far away from bond rupture events (blue region), with the ReaxFF reactive force field used to describe the rupture processes at the crack tip (yellow region). (b) The results of a computational experiment with a slowly increasing mode I load, for the (111) oriented crystal. The strain rate is 0.0005% strain increment per 1.5 fs integration step. The initial, static regime is followed by a short period of crack growth during which a perfectly flat, mirror-like surface is generated. Crack propagation becomes increasingly erratic until the entire crystal is fractured.

reactive force field[20,35,36] with a Tersoff potential[37]. This method is based on the strategy of integrating a set of computational tools, as outlined in Fig. 3. Atomistic simulations of such fracture processes provide a fundamental insight into the details of crack extension[20]. For instance, the simulations[21] reveal that the steady-state fracture speed has a minimum threshold speed of approximately 2 kms^{-1}, a finding in agreement with earlier experimental studies[38].

Hierarchical BPMs

The two previous examples highlight two prominent mechanisms of deformation in crystalline materials: dislocation nucleation and brittle crack extension. In this section, we discuss how the understanding that exists for crystalline systems can be extended to biological materials.

BPMs have a significantly different molecular structure than crystalline materials, which induces a variety of novel deformation

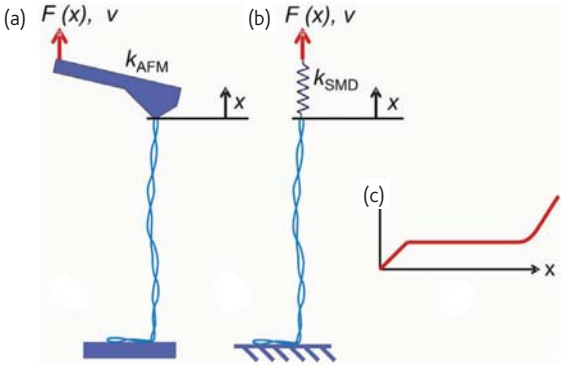

Fig. 6 Single-molecule pulling experiments carried out on a coiled-coil (CC) protein structure. (a) An experimental setup based on AFM, and (b) a steered molecular dynamics (SMD) analogue. In the SMD approach, the end of the molecule is slowly pulled at a pulling velocity v vector. This leads to a slowly increasing force $F = k(v \cdot t - x)$ ($k = 10$ kcal/mol/Å^2), where t is the time and x is the current position vector of the end of the molecule (F(x), schematically shown in (c)). Both approaches, AFM and SMD, lead to force displacement information. In addition to the F(x) curve, SMD provides detailed information about associated atomistic deformation mechanisms. Because of the time scale limitations of MD to several nanoseconds, there is typically a large difference between simulation and experiment with respect to pulling rates. Whereas MD simulations are limited to pulling rates of ≈ 0.1 ms^{-1}, experimental rates are six to eight magnitudes smaller. This requires additional consideration in order to interpret MD results in light of experimental findings.

mechanisms. Understanding these mechanisms poses a very challenging set of problems. Furthermore, the application of the insight from such studies to address significant biological and biomedical questions or to suggest new biomimetic material designs are exciting intellectual and interdisciplinary opportunities.

Atomistic modeling of protein materials

All MD simulations reviewed here have been performed at a temperature of 300 K (NVT ensemble), with temperature control using a Berendsen thermostat[22] and a time step of 1 fs. In all cases, the molecular structure obtained from the Protein Data Bank is solved completely in a water skin that encompasses the entire protein structure. Careful energy minimization and finite temperature equilibration of all structures are simulated before the protein is deformed. We use visual molecular dynamics (VMD) for visualization of protein structures[39] and MD simulations are carried out using NAMD[40] with the CHARMM22 force field with explicit TIP3 water[41].

To apply forces to the molecule, we use steered molecular dynamics (SMD)[12]. The SMD technique is equivalent to attaching one end of a virtual harmonic spring to the end of the system and pulling at the virtual atom on the other end of the spring, with a pulling speed v. The SMD method mimics an experiment where one end of the molecule is fixed (e.g. on a Au surface), while the other end is pulled with an AFM cantilever tip (see Fig. 6). The molecular strain is defined as $\varepsilon = (x - x_0)/x_0$, where x_0 is the undeformed length and x is the deformed length of the protein structure.

Extended Bell theory: theoretical nanomechanics of protein materials

The key to comprehend the mechanical response of BPMs across different time and length scales is to understand the rupture mechanics of HBs under laterally applied load. Typically, a variety of unfolding processes exist for a protein structure, each of which has a specific reaction pathway and an associated energy barrier, mostly related to the underlying bond-breaking mechanisms and rearrangements in the protein structure. Several theories exist that describe competing processes arising from mechanically induced instabilities of protein

Extended Bell theory

Whereas continuum theories are suitable to describe the deformation of macroscopic structures, statistical concepts must be employed to accurately model the mechanical behavior of protein structures. Bell's theory is one of the most widely used models to describe the statistical nature of bond breaking.

In Bell's theory[42–46], the off rate χ is the product of the natural bond vibration frequency ω_0 and the quasi-equilibrium likelihood of reaching the transition state with an energy barrier E_b that is reduced by mechanical energy $F \cdot x_b \cdot \cos(\theta)$, where F is the applied force, x_b is the distance between the equilibrated state (minimum of the well) and the transition state, and θ is the angle between the direction of the reaction pathway of bond breaking (x-direction) and the direction of applied load F (see Fig. 7). The angle can be determined by analyzing the molecular geometry. The off rate is given by:

$$\chi = \omega_0 \cdot \exp\left(-\frac{(E_b - F \cdot x_b \cdot \cos(\theta))}{k_b \cdot T}\right) \quad (1)$$

and describes how often a bond is broken per unit time (it equals the reciprocal of the lifetime of a bond). The natural vibration frequency of a bond[46] is $\omega_0 \approx 1 \times 13\ s^{-1}$.

However, eq 1 does not describe the dependence of the pulling speed (the controlled parameter in experiment and MD simulation) at which a bond breaks because of the applied pulling force. Instead, it only provides an estimate of the time scale at which the bond will be broken. In order to overcome this limitation, we modify eq 1 based on the following idea: the speed ν at which a bond is broken equals the distance that needs to be overcome in order to break the bond (x_b) divided by the time for bond breaking. Consequently, ν is the product of $\chi \cdot x_b$. This leads to the following equation for the bond breaking speed[47]:

$$v = \omega_0 \cdot x_b \cdot \exp\left(-\frac{(E_b - F \cdot x_b \cdot \cos(\theta))}{k_b \cdot T}\right) \quad (2)$$

This equation can be rewritten in the following way:

$$v = v_0 \cdot \exp\left(\frac{F \cdot x_b \cdot \cos(\theta)}{k_b \cdot T}\right) \quad (3)$$

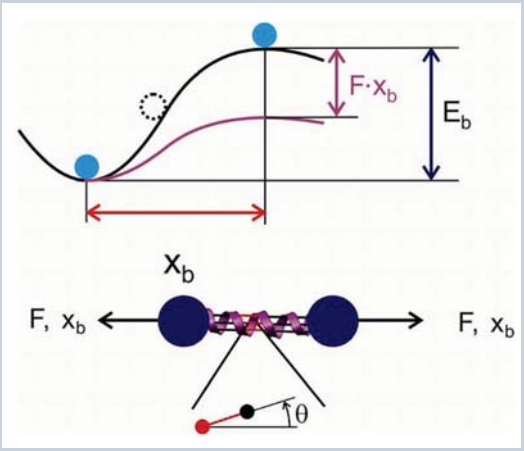

Fig. 7 Statistical theory to predict the bond rupture mechanics. The graph depicts the energy as a function of deformation along a deformation variable (upper plot), along a particular pathway that leads to bond rupture; where F is the applied force and x_b is the displacement in the direction of the applied force. In the schematic, three HBs (indicated by the red color, lower plot) break simultaneously. Thus, x_b corresponds to the lateral displacement that is necessary to overcome the bond breaking distance of a HB, in the particular atomistic geometry present in the CC. Given that x_b^* is the distance to break a single HB, the distance $x_b^* = x_b \cos\theta$ denotes the lateral displacement at bond breaking, with the angle as the angle θ between pulling direction and orientation of the HB inside the molecule.

with ν_0 as the natural bond breaking speed (when no load is applied), defined as:

$$v_0 = \omega_0 \cdot x_b \cdot \exp\left(-\frac{E_b}{k_b \cdot T}\right) \quad (4)$$

This modified framework enables us to study the dependence between the unfolding force and the bond breaking speed or to calculate the average force at which a bond breaks, at a certain pulling rate. We can rewrite eq 3 as:

$$F(v) = \frac{k_b \cdot T}{x_b \cdot \cos(\theta)} \cdot \ln v - \frac{k_b \cdot T}{x_b \cdot \cos(\theta)} \cdot \ln v_0 = a \cdot \ln v + b \quad (5)$$

where $a = k_b \cdot T/(x_b \cdot \cos\theta)$ and $b = -k_b \cdot T/(x_b \cdot \cos\theta) \cdot \ln \nu_0$. Eq 5 predicts that the unfolding force depends logarithmically on the pulling speed in a nonequilibrated system. We note that it contains two parameters a and b, which can be calculated from the parameters x_b and E_b at a certain temperature and angle. The concept is summarized in Fig. 7.

structures. These concepts stem primarily from a theory originally postulated by Bell in 1978[42–46].

Eq. 5 (see text box) provides an immediate link between the molecular geometry (via the angle θ), the pulling rate, and the pulling force *F* that is necessary to lower the energy barrier in such a way that the HBs can be broken at the applied pulling velocity.

A possible strategy to determine the dependence of the unfolding force *F* on pulling speed, associated mechanisms, and energy barriers is to carry out MD simulations at different pulling rates, measure the dependence of unfolding force on the pulling rate, and fit the parameters *a* and *b* to this data. This information can then be used to calculate the parameters x_b and E_b and thereby reconstruct the free energy landscape.

Biological role of vimentin IFs

Together with globular protein microtubules (MTs) and microfilaments (MFs), IFs are one of the three major components of the cytoskeleton in eukaryotic cells[48]. The cytoskeleton plays a critical role not only in determining the shape and the mechanical properties of the cell, but is also vital for many additional functions including protein synthesis, cell motility, and cell division or wound healing[48–50]. Here we focus on the mechanical behavior of vimentin IFs. Fig. 8 displays the hierarchical structure of vimentin networks, from the molecular to the cellular level.

Vimentin IFs have a variety of functions on several hierarchical levels. On the cellular scale, vimentin networks act primarily as the 'security belts' of the cell[51]. Because of their architecture, the flexible networks are very soft at small deformations and pulling rates, leading to 'invisibility' and nonresistance during cell movement. Conversely, very stiff behavior is observed at large deformation and high deformation rates, ensuring their function on the cellular as well as on the tissue level[49]. The mechanical role of IFs is particularly evident in diseases in which the loss of mechanical function and integrity of various tissues is associated with intermediate-filament-protein mutations, as reviewed elsewhere[52,53].

Recently, additional functions have been found on the subnetwork filament level, which control the location, shape, and stability of cell organelles (e.g. mitochondria or golgi), their function, and the protein targeting process[54]. Yet other functions exist on the molecular level, consisting of different regulation mechanisms such as cell signaling (e.g. transcriptional effects, mechanotransduction), or associated protein organization (e.g. plectin or chaperones)[54,55].

Large deformation behavior of vimentin IFs

Here we focus on the large deformation behavior of vimentin proteins[4,48,56,57]. When cells and thus entire IF networks are deformed, each vimentin filament undergoes a tensile deformation, which

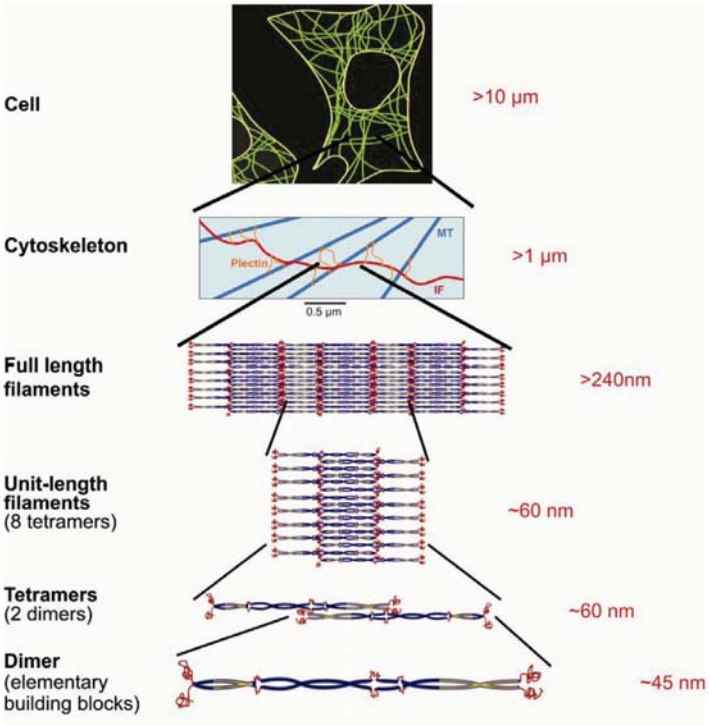

Fig. 8 Hierarchical structure of the IF network in cells. Through carefully following the various steps of assembly[72,77] it has been shown that dimers associate to fibrils, which form the second level of the hierarchy. In vivo, these fibrils can reach a length of up to several microns and consist of 16 dimers in cross section. The third level of hierarchy consists of three-dimensional IF networks inside the cell, reinforcing the plasma membrane[49,60,61]. Inside the network, IF-associated proteins such as plectins generate the connection between individual IFs as well as between other cytoskeletal components. The characteristic loading condition of full length filaments is tensile loading. Because of this tensile load, each dimer is subject to a tensile load if the cell undergoes large deformation.

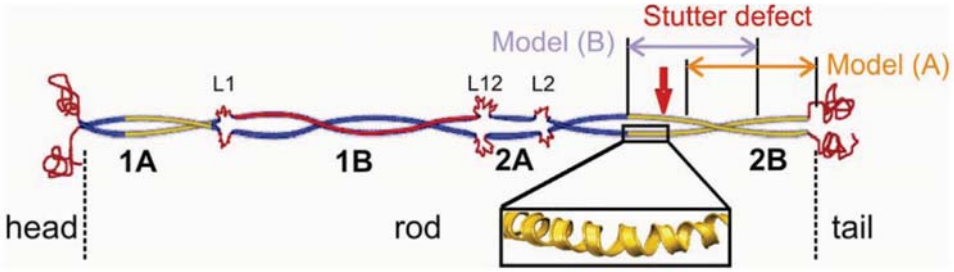

Fig. 9 Geometry of the molecular building block of vimentin. The dimers, approximately 45 nm long, are the elementary building blocks of vimentin IFs. A dimer consists of a head, tail (plotted in red), and an elongated rod domain that is divided into four alpha-helical CCs (1A, 1B, 2A, 2B) connected through linkers L1, L12, L2 (also red)[78]. We also indicate the segments of the dimer that correspond to the CC without stutter (model A) and the CC with stutter defect (model B).

is carried by individual dimers at the molecular level. Therefore, a detailed understanding of coiled-coil (CC) dimers and their mechanical properties under small and large tensile deformations is vital to provide insight into the function and mechanisms of vimentin filaments and networks[49,58–61]. Fig. 9 depicts the molecular geometry of the CC dimer. The following simulations are carried out by stretching a short segment in the 2B domain of the dimer, as indicated in the schematic.

Fig. 10 depicts force-strain curves of an IF CC dimer, at different pulling rates, obtained by MD simulations[47,62–64]. The force-extension curves depend strongly on the pulling velocity. Fig. 11a depicts the unfolding force, which determines the force level during the second regime, as a function of pulling speed. These results clearly confirm the logarithmic dependence of the unfolding force on the pulling speed, as predicted by the extended Bell theory (eq 5). MD simulations in the fast pulling regime show that E_b = 5.59 kcal mol^{-1} and x_b = 0.185 Å,

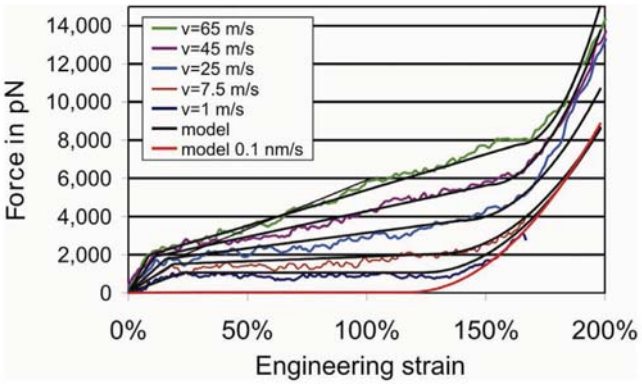

Fig. 10 Force-strain curves for mechanical tensile deformation of a CC vimentin dimer[47]. The continuous curves represent results obtained from a theoretical model based on the Bell theory that enables one to predict the unfolding mechanics for a wide range of pulling velocities. The first regime represents elastic deformation, up to approximately 10–25% tensile strain. This regime is followed by a plateau region during which unfolding of the CC structure occurs at approximately constant force level. The last regime displays significant strain hardening, during which the coiled superhelix is lost and the protein backbone is stretched, leading to a significant increase in stiffness.

with θ = 23° ± 10.2°, suggesting that the unfolding mechanism is characterized by sequential breaking of single HBs[47] (this is concluded since the energy for a single HB is in the range of 5 kcal mol^{-1}).

It has been found that deformation mechanisms depend on the pulling speed[47], and that there is a change in deformation mechanism

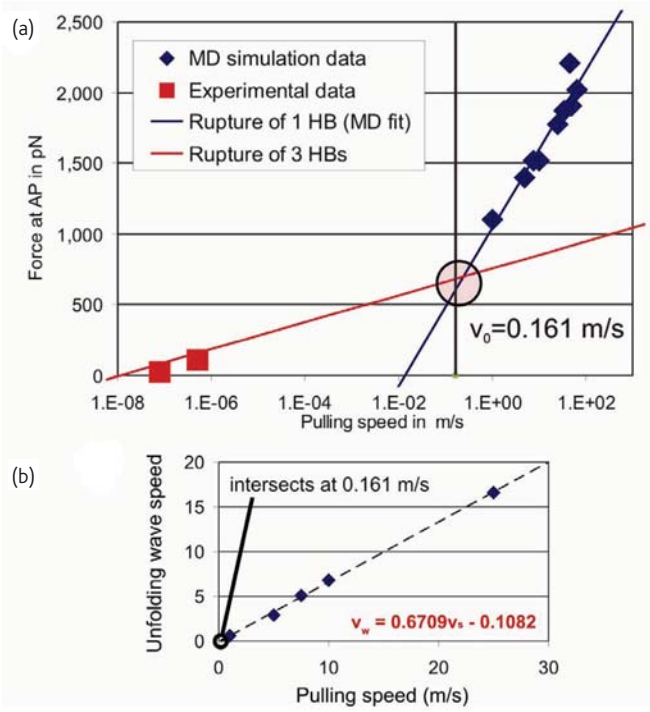

Fig. 11 (a) Unfolding force of a vimentin dimer (at the angular point), as a function of the pulling velocity[47]. All simulation results display a logarithmic dependence of the unfolding force on the pulling velocity, in agreement with the predictions by the extended Bell theory. (b) Unfolding wave speed as a function of lateral pulling speed. The unfolding wave is predicted to disappear at a pulling velocity of approximately 0.161 ms^{-1}; this leads to a change of strain distribution from localization of strain at the ends of the molecule to a homogeneous strain along the molecular axis. This induces a different molecular unfolding mechanism, which is characterized by breaking of three HBs, at a lateral applied displacement of ≈ 1.25 Å. The second regime is plotted in (a) as a red line. The predictions based on this model agree well with experimental results.

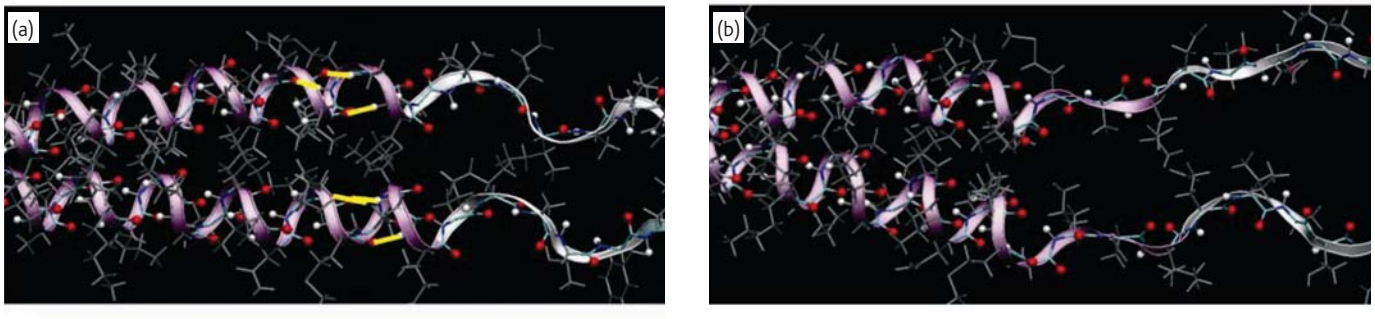

Fig. 12 Visualization of the atomistic-scale unfolding process of the CC structure. The yellow lines in (a) indicate the HB that forms between the backbone O atom and the H atom connected to the N atom in the protein backbone, and which have broken in (b). The unfolding wave destroys these HBs, leading to loss of the helical structure.

because of a change in strain distribution. At large pulling velocities, an 'unfolding wave' propagates throughout the molecule, sequentially breaking HBs one by one. Physically, the unfolding wave represents a localization of strain that leads to the local rupture of HBs before the entire protein is equilibrated. As shown in Fig. 11b, the speed of this unfolding wave reaches zero at a pulling speed of 0.161 ms^{-1}. Thus, at lower pulling rates, this localization of strain in a convolution does not occur – since there is no unfolding wave – and all HBs in a convolution are stretched equally. Failure then occurs by simultaneous rupture of three HBs in one arbitrary convolution of the alpha helix (AH).

Thus, in order to apply the extended Bell theory (eq 6) to the slow pulling regime, the parameters E_b and x_b must be modified. We multiply E_b by a factor of three to account for the fact that three HBs rupture simultaneously instead of one, and use a value for x_b of 1.25 Å (corresponding to the transition distance of HBs[47]). We plot the prediction according to this model in Fig. 11a. A comparison with experiments[52,65] reveals reasonable agreement.

Fig. 12 depicts details of the atomistic rupture mechanisms as the CC structure is unfolded. Fig. 13a displays the overall molecular unfolding dynamics. We note that the intersection of the unfolding force corresponding to the two modes is very close to the predicted transition speed of 0.161 ms^{-1}. This provides an independent confirmation of the hypothesis[47].

Molecular defects in vimentin dimers: soft spots

A variety of discontinuities or 'defects' exist that interrupt the CC periodicity locally without destroying the overall molecular structure. 'Skips' are insertions of one residue into the heptad pattern (a characteristic seven residue repeat in CCs)[66], 'stammers' result through an insertion of three additional residues[67–69], and 'stutters'

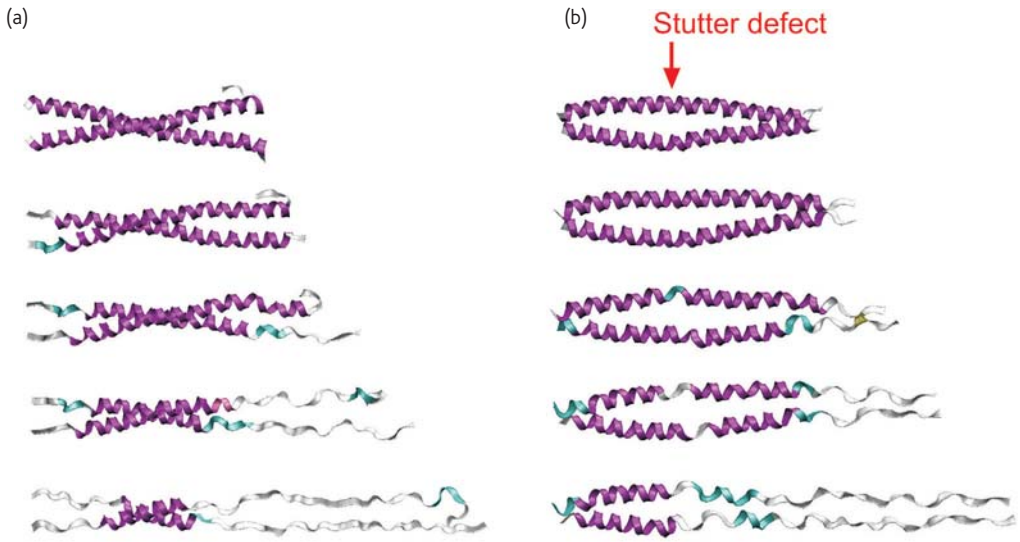

Fig. 13 Snapshots of the unfolding dynamics, (a) for a perfect CC, corresponding to model A in Fig. 9, and (b) the CC with the stutter domain, corresponding to model B in Fig. 9[64]. Unfolding proceeds sequentially, beginning from the end where the load is applied. It is apparent that the stutter represents a location where unfolding starts as well (see the 2nd and 3rd snapshot from the top, where it is evident that the AH motif begins to disappear at the location of the stutter). The red arrow indicates the location of the stutter. The structure is rendered using the VMD ribbons method; color is assigned according to the secondary protein structure (thus loss of the AH structure is visible by change towards a white color). The initial length of both structures is 70 Å.

appear if four additional residues interrupt the heptad sequence[70]. Presence of a stutter results in an almost parallel run of both AHs without interrupting the CC geometry. To date, little is known about the biological, mechanical, or physical reasons for the presence of these molecular defects. It has been shown recently that mutations in desmin IFs related to different myopathies – effectively leading to muscle weakness – result in additional stutters or even the creation of stammers in the dimer structure[71]. Vimentin dimers have a highly conserved stutter in the 2B segment of the dimer, as shown in Fig. 9.

Based on analysis of the geometry of the CC structure, the extended Bell theory predicts that the stutter represents a molecular defect at which unfolding occurs at lower forces than in the rest of the protein. Geometrically, the difference of a perfect CC and the segment that includes the stutter region is the angle θ. In the perfect CC, the angle θ_{cc} = 23° ± 10.2°, whereas within the stutter region, the angle θ_{St} = 16° ± 8.5° (the angle $\theta_{St} \neq 0°$ since the HBs of a straight AH are slightly tilted in the direction of the twisting backbone).

Provided that x_b and E_b are equal – that is, assuming the same unfolding mechanism – the extended Bell theory predicts that the structure with the larger angle is stronger (for $\theta_2 > \theta_1$, $\cos\theta_2 < \cos\theta_1$):

$$F_2(v) = \frac{\cos\theta_1}{\cos\theta_2} \cdot F_1(v) \qquad (6)$$

Therefore, in a system that consists of a combination of a perfect CC and a stutter defect, the stutter defect represents the weakest segment, which will unfold most easily under increasing applied tensile load. The MD simulation results shown in Fig. 13b confirm this hypothesis, as they show that the CC unfolds at the stutter region.

Introducing the stutter into the dimer structure thus corresponds to the deliberate addition of a weakening 'defect' into the molecular structure. The biological role of the stutter may be to provide a predefined, and, most importantly, controlled location where unfolding occurs under large deformation. As pointed out above, vimentin IFs have their most significant role in large deformation behavior.

Supermolecular deformation mechanisms of tetramers

The studies reviewed in the previous sections were performed at the molecular level. Here we provide a simple analysis of the deformation mechanisms at the next highest scale, describing the interaction between two dimers.

The analysis of the nanomechanics of a vimentin dimer reveals that at pulling velocities that range between 1 x 10^{-8} ms^{-1} and 1 x 10^{-6} ms^{-1} (rates that appear *in vivo* and in experiments), the unfolding force of the CC structure is predicted to range between approximately 50 pN and 200 pN. This estimate for the unfolding force enables elucidation of the deformation mechanism of a tetramer structure, that is, the combination of two dimers (see Fig. 8). Experimental analyses of the assembly processes suggest that assembly of two dimers occurs via the interaction of the head and tail domains with the CC structure, as shown in Fig. 14a[60,72].

Here we present a simple analysis considering the random coil domain of the head as an entropic chain, modeled using the worm-like chain (WLC) theory[73] (see Fig. 14b). The model reveals that that

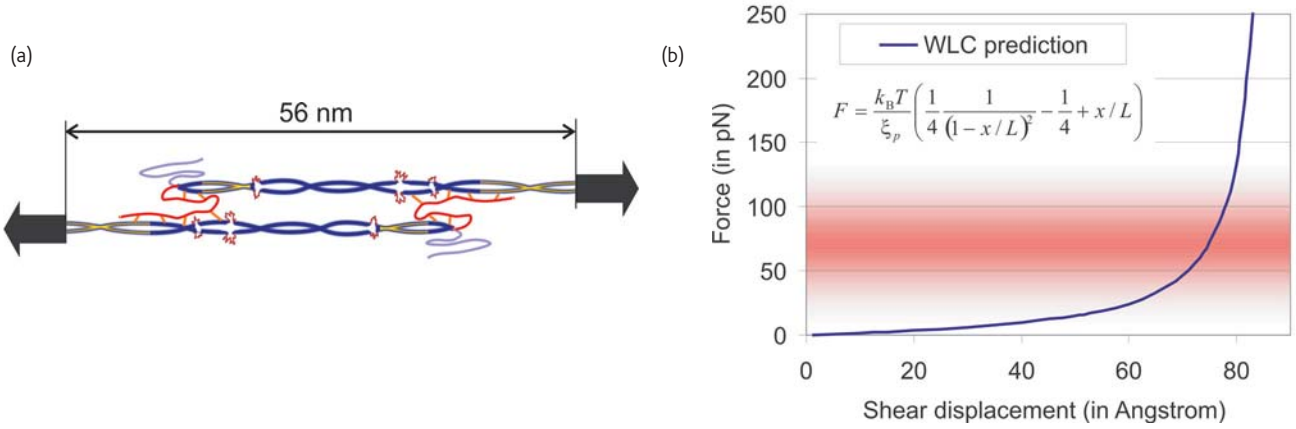

Fig. 14 (a) Assembly of two dimers into a tetramer (see also Fig. 9). (b) The interaction between two dimers is considered as a random coil polypeptide chain and modeled with the WLC theory (see inset equation, where $\xi_p \approx 0.4$ nm is the persistence length of a single polypeptide, x the end-to-end distance, and L the contour length). We assume that 1/3 of the ≈ 80 residues are not bonded to either of the two molecules, and thus deform according to entropic elasticity, defining L. This simple analysis reveals that that unfolding of the dimer begins when the shear displacement ranges between 70 Å and 80 Å (note that the interdimer shear force induced by the two entropic chains combined reaches the range of the critical CC unfolding force between 25 pN and 100 pN, marked here with the red shaded area). This simple analysis predicts a change in deformation mechanism from entropic dominated elastic stretching of the head/tail domains to uncoiling of the CC structures.

unfolding of the dimer begins when the shear displacement between the molecules equals between 70 Å and 80 Å, or, equivalently, between 12% and 14% tensile strain, because at this point the resistance induced by the random coil then reaches the force necessary to induce unfolding of the CC structure (see Fig. 11). We emphasize that this is a simple calculation. However, it clearly illustrates that entropic elasticity can lead to forces that are sufficiently large to induce unfolding of the protein structure.

This analysis suggests a possible change in the deformation mechanism from entropic-dominated elastic stretching of the head/tail domains to uncoiling of the CC structures. This is an example of concurrent mechanisms that operate at different scales. On the one hand, there is rupture of HBs on the dimer scale; on the other hand, there are entropic effects between dimers on the supermolecular level. This particular molecular architecture effectively results in controlled yield over hundreds of percent of strain. We emphasize that the understanding of these mechanisms is currently only in its infancy, in particular the competition between intermolecular adhesion, entropic elasticity, and molecular unfolding.

Discussion and conclusion

Deformation and fracture are intimately linked to the atomic microstructure of the material. Whereas crystalline materials show mechanisms such as dislocation spreading or crack extension

Table 1 Selection of various material defects, their appearance, and how they control the deformation and fracture properties.

Defect	Description	Materials in which defect is found	Consequences for mechanics	Remarks
Crack	Void-like inclusion or surface crack; region with reduced traction across a molecular plane	Many crystals (metals, ceramics), in tissues (larger scales > several micrometers)	Location of stress concentration; applied stress is multiplied many times at a crack tip; can lead to breaking or shearing of atomic bonds	Cracks at various scales largely control the strength of crystalline materials
Dislocation	Localized shear displacement in crystals	Predominantly metals and other crystalline materials	Mediates plastic deformation	Nucleation of dislocations often competes with crack extension; determines whether a material is brittle or ductile
Modifications in secondary protein structure, e.g. stutter defect in CCs	Two AHs in CC run in parallel, thus loss of helical geometry	BPMs with distinct secondary structure, e.g. IFs	Weaker molecular structure, unfolds first under load	Stutter defect provides a means to control unfolding locations with molecular precision.
Amino acid sequence mutation	Replacement, deletion or addition of a specific amino acid	Any protein based material	May strengthen or weaken the material	Some mutations lead to diseases; other mutations are necessary to improve the function (e.g. antibodies are generated through random mutations and thus enable resistance)
Grain boundary (GB)	Interface between two differently oriented crystals	Crystalline materials (metals, ceramics)	Mediates deformation, e.g. by GB sliding, GB diffusion at high temperatures	GBs are particularly important at small grain sizes, e.g. nanocrystalline metals
Vacancy	Missing atom in crystal lattice	Crystalline materials	Enhances diffusive material transport, which mediates deformation	Critical for high-temperature material behavior
Craze	Region of localized yielding, formation of microvoids and fibrils	Polymers, plastics	Process prior to cracking, dissipates energy	Increases toughness of plastics
Shear band	Small region inside material in which localized shear has occurred	Polymers, metallic glasses	Reduction of the material strength	Mediates plasticity

(Figs. 4 and 5), hierarchical BPMs feature molecular unfolding or sliding, where HB rupture is of particular significance (see Figs. 2 and 12). The dominance of specific mechanisms is controlled by geometrical parameters as well as by the structural arrangement of the protein elementary building blocks across many hierarchical scales, from nano to macro (Figs. 1 and 2). It is known that nano- or microscopic structures often control the macroscopic material behavior: for example, grain size reduction or confinement leads to an increase of the strength in crystalline metals[30,74–76]. Similar mechanisms are observed in biological materials. For instance the alteration of the molecular length of tropocollagen molecules in collagen fibrils directly controls the dominating deformation mechanism and influences the strength[6,15].

A major trait of BPMs is the occurrence of hierarchies and the abundance of weak interactions. The presence of hierarchies in biological materials may be vital to take advantage of molecular and submolecular features, often characterized by weak interactions, and multiply their properties so that they become visible at larger scales. Use of weak interactions makes it possible to produce strong materials at moderate temperatures and thus with limited energy use. Weak interactions are also critical for controllability, since their formation and rupture can be directed by changes in the chemical environment at minimal energy use. Cells or organisms maintain control over structural assemblies based on such bonds. Controllability is vital in the context of complex biological signaling pathways.

Another distinction between traditional and biological materials is the geometrical occurrence of defects. While defects are often distributed randomly over the volume in crystalline materials, biological materials consist of an ordered structure that reaches down to the nanoscale. Defects are placed with atomistic or molecular precision, and may play a major role in the material behavior observed at larger scales. In IF, the addition of molecular stutter defects leads to soft spots that represent preferred locations of protein unfolding[64].

These results suggest that analogies can be drawn between biological and synthetic materials. Table 1 summarizes a few crystal and molecular defects, their impact on the deformation behavior and how they control the material properties.

In addition to the long-term impact in biology, bioengineering, and medicine, this research may eventually contribute to our understanding of how different scales interact with one another.

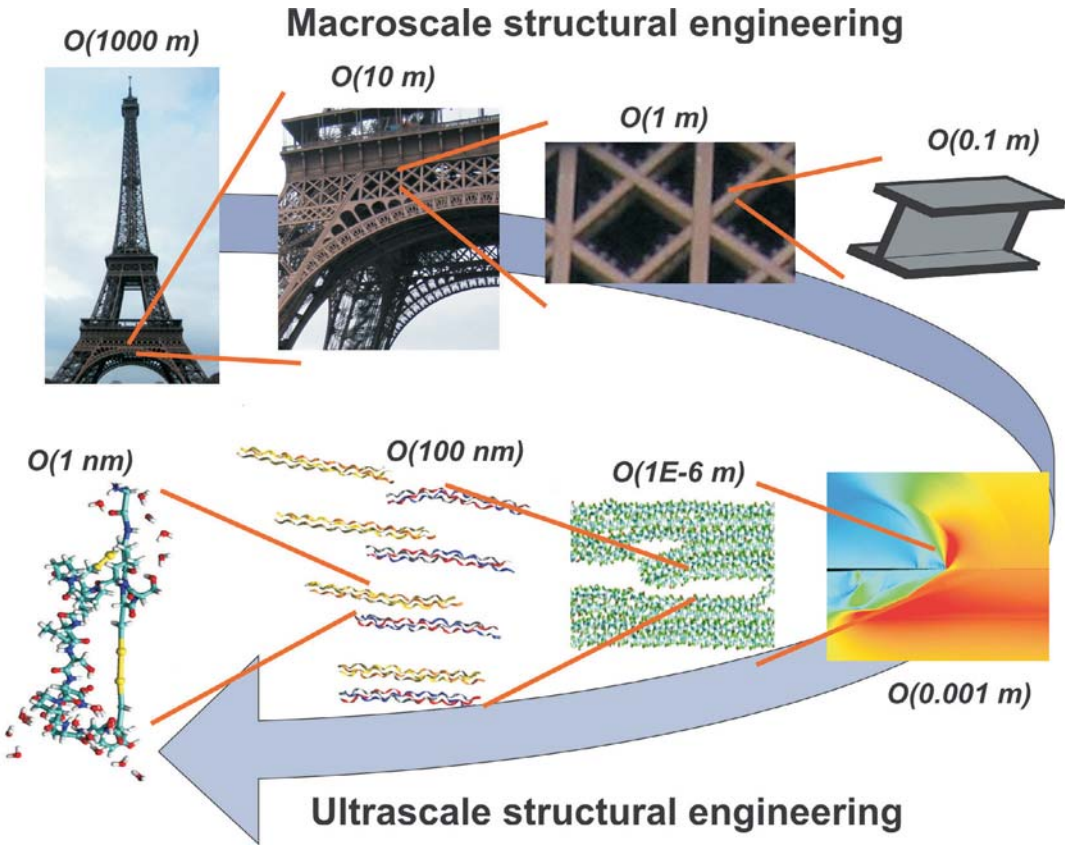

Fig. 15 The long term impact of our work is that it will extend our ability to perform structural engineering at the macroscale, to the ultimate scale, the nanoscale. Opening the material scale as design space for new material development may open endless possibilities for development of robust, adaptive, active, and 'smart' materials.

It may also enable synthesis of novel complex structural materials, designed from the nano- to the macroscale, as shown in Fig. 15. In order to achieve these goals, major challenges must be overcome, in particular in relating molecular processes to larger-scale phenomena. As illustrated in Fig. 8, protein materials constitute exceedingly complex structures. While the behavior of individual proteins is reasonably well understood, the properties of large assemblies of proteins remain largely unknown. mt

Acknowledgments

This research was partly supported by the Army Research Office (ARO), grant number W911NF-06-1-0291 (program officer Bruce LaMattina), as well as a National Science Foundation CAREER Award, grant number CMMI-0642545 (program director Jimmy Hsia). TA acknowledges the support of the German National Academic Foundation and the Juergen-Ulderup Foundation. We acknowledge discussions with Harald Herrmann (University of Heidelberg, Germany) and Laurent Kreplak (University of Basel, Switzerland), as well as continued support by Lothar Gaul (University of Stuttgart, Germany).

REFERENCES

1. Broberg, K. B., *Cracks and Fracture*, Academic Press, London, (1990)
2. Courtney, T. H., *Mechanical behavior of materials*, McGraw-Hill, New York, (1990)
3. Hirth, J. P., and Lothe, J., *Theory of Dislocations*, Wiley, New York, (1982)
4. Alberts, B., *et al.*, *Molecular Biology of the Cell*, Garland, New York, (2002)
5. Buehler, M. J., *J. Mater. Res.* (2006) **21**, 1947
6. Buehler, M. J., *Proc. Natl. Acad. Sci. USA* (2006) **103**, 12285
7. Fratzl, P., *et al.*, *J. Mater. Chem.* (2004) **14**, 2115
8. An, K.-N., *et al.*, *Biorheology* (2004) **41**, 239
9. Ramachandran, G. N., and Kartha, G., *Nature* (1955) **176**, 593
10. Buehler, M. J., *Nanotechnology* (2007) **18**, 295102
11. Freund, L. B., *Dynamic Fracture Mechanics*, Cambridge University Press, Cambridge (1990)
12. Lu, H., *et al.*, *Biophys. J.* (1998) **75**, 662
13. Rief, M., *et al.*, *Science* (1997) **276**, 1109
14. Fantner, G. E., *et al.*, *Nat. Mater.* (2005) **4**, 612
15. Buehler, M. J., *J. Mech. Behavior Biomed. Mater.* (2007), doi: 10.1016/j.jmbbm.2007.04.001
16. Buehler, M. J., and Wong, S. Y., *Biophys. J.* (2007) **93**, 37
17. Engler, A. J., *et al.*, *Cell* (2006) **126**, 677
18. Buehler, M. J., and Gao, H., *Nature* (2006) **439**, 307
19. Buehler, M. J., *et al.*, *Nature* (2003) **426**, 141
20. Buehler, M. J., *et al.*, *Phys. Rev. Lett.* (2006) **96**, 095505
21. Buehler, M. J., *et al.*, Threshold crack speed in dynamic fracture of silicon, In *Multiscale Modeling of Materials*, Devanathan, R., *et al.*, (eds.), Mater. Res. Soc. Symp. Proc., Warrendale, USA (2007), **978E**, 0978-GG02-03
22. Allen, M. P., and Tildesley, D. J., *Computer Simulation of Liquids*, Clarendon Press, New York, (1989)
23. Goddard, W. A., A Perspective of Materials Modeling. In *Handbook of Materials Modeling*, Yip, S., (ed.), Springer, Berlin, (2005)
24. Tai, K., *et al.*, *Nano Lett.* (2006) **6**, 2520
25. Sun, Y.-L., *et al.*, *J. Biomech.* (2004) **37**, 1665
26. Dao, M., *et al.*, *J. Mech. Phys. Solids* (2005) **53**, 493
27. Lim, C. T., *et al.*, *Mater. Sci. Eng., C* (2006) **26**, 1278
28. Daw, M. S., and Baskes, M. I., *Phys. Rev. B* (1984) **29**, 6443
29. Angelo, J. E., *et al.*, *Modell. Simul. Mater. Sci. Eng.* (1995) **3**, 289
30. Wolf, D., *et al.*, *Metallkunde* (2003) **94**, 1052
31. Van Swygenhoven, H., *et al.*, *Nat. Mater.* (2004) **3**, 399
32. Yamakov, V., *et al.*, *Nat. Mater.* (2004) **3**, 43
33. Rice, J. R., and Thomson, R. M. *Philos. Mag.* (1974) **29**, 73
34. Rice, J. R., *J. Mech. Phys. Solids* (1992) **40**, 239
35. van Duin, A. C. T., *et al.*, *J. Phys. Chem. A* (2001) **105**, 9396
36. van Duin, A. C. T., *et al.*, *J. Phys. Chem. A* (2003) **107**, 3803
37. Tersoff, J., *Phys. Rev. Lett.* (1988) **61**, 2879
38. Hauch, J. A., *et al.*, *Phys. Rev. Lett.* (1999) **82**, 3823
39. Humphrey, W., *et al.*, *J. Mol. Graphics* (1996) **14**, 33
40. Nelson, M. T., *et al.*, *Int. J. Supercomputer Appl. High Performance Computing* (1996) **10**, 251
41. MacKerell, A. D., Jr., *et al.*, *J. Phys. Chem. B* (1998) **102**, 3586
42. Evans, E., and Ritchie, K., *Biophys. J.* (1997) **72**, 1541
43. Dudko, O. K., *et al.*, *Phys. Rev. Lett.* (2006) **96**, 108101
44. Wiita, A. P., *et al.*, *Proc. Natl. Acad. Sci. USA* (2006) **103**, 7222
45. Gilli, P., *et al.*, *J. Am. Chem. Soc.* (2004) **126**, 3845
46. Bell, G. I., *Science* (1978) **200**, 618
47. Ackbarow, T., and Buehler, M. J., *J. Mater. Sci.* (2007) doi: 10.1007/s10853-007-1719-2
48. Wang, N., and Stamenovic, D., *J. Muscle Res. Cell Motil.* (2002) **23**, 535
49. Mücke, N., *et al.*, *J. Mol. Biol.* (2004) **335**, 1241
50. Helfand, B. T., *et al.*, *J. Cell Sci.* (2004) **117**, 133
51. Burkhard, P., *et al.*, *Struct. Folding Design* (2000) **8**, 223
52. Kiss, B., *et al.*, *J. Struct. Biol.* (2006) **155**, 327
53. Omary, M. B., *et al.*, *N. Engl. J. Med.* (2004) **351**, 2087
54. Toivola, D. M., *et al.*, *Trends Cell Biol.* (2005) **15**, 608
55. Bruck, H. A., *et al.*, *Exp. Mech.* (2002) **42**, 361
56. Janmey, P. A., *et al.*, *J. Cell Biol.* (1991) **113**, 155
57. Schietke, R., *et al.*, *Eur. J. Cell Biol.* (2006) **85**, 1
58. Moir, R. D., and Spann, T. P., *Cell. Mol. Life Sci.* (2001) **58**, 1748
59. Wilson, K. L., *et al.*, *Cell* (2001) **104**, 647
60. Herrmann, H., and Aebi, U., *Annu. Rev. Biochem.* (2004) **73**, 749
61. Strelkov, S. V., *et al.*, *J. Mol. Biol.* (2004) **343**, 1067
62. Ackbarow, T., and Buehler, M. J., Hierarchical nanomechanics of vimentin alpha helical coiled-coil proteins. In *Multiscale Modeling of Materials*, Devanathan R., *et al.*, (eds.), Mater. Res. Soc. Symp. Proc., Warrendale, USA (2007), **978E**, 0978-GG10-05
63. Ackbarow, T., and Buehler, M. J., unpublished results
64. Ackbarow, T., and Buehler, M. J., unpublished results
65. Schwaiger, I., *et al.*, *Nat. Mater.* (2002) **1**, 232
66. McLachlan, A. D., and Karn, J., *J. Mol. Biol.* (1983) **164**, 605
67. Brown, J. H., *et al.*, *Proteins: Struct., Funct., Genet.* (1996) **26**, 134
68. Strelkov, S. V., *et al.*, *EMBO J.* (2002) **21**, 1255
69. Herrmann, H., and Aebi, U., *Cell. Mol. Life Sci.* (1999) **55**, 1416
70. Parry, D. A. D., *J. Mol. Biol.* (1978) **120**, 545
71. Kaminska, A., *et al.*, *Hum. Genet.* (2004) **114**, 306
72. Kreplak, L., *et al.*, *Exp. Cell Res.* (2004) **301**, 77
73. Bustamante, C., *et al.*, *Science* (1994) **265**, 1599
74. Yip, S., *Nature* (1998) **391**, 532
75. von Blanckenhagen, B., *et al.*, *Modell. Simul. Mater. Sci. Eng.* (2001) **9**, 157
76. Nieh, T. G., and Wadsworth, J., *Scripta Metall. Mater.* (1991) **25**, 955
77. Smith, T. A., *et al.*, *Proteins: Struct., Funct., Genet.* (2003) **50**, 207
78. Strelkov, S. V., *et al.*, *Bioessays* (2003) **25**, 243